

Synthesis of redox-active $\text{Ce}_{0.75}\text{Bi}_{0.15}\text{Tb}_{0.1}\text{F}_3$ nanoparticles and their biocompatibility study *in vitro*

Nikita N. Chukavin^{1,a}, Danil D. Kolmanovich^{1,b}, Arina D. Filippova^{2,c}, Maria A. Teplonogova^{2,d}, Vladimir K. Ivanov^{2,e}, Anton L. Popov^{1,f}

¹Institute of Theoretical and Experimental Biophysics of the Russian Academy of Sciences, 142290, Russia

²Kurnakov Institute of General and Inorganic Chemistry of the Russian Academy of Sciences, Moscow, 119991, Russia

^achukavinnik@gmail.com, ^bkdd100996@mail.ru, ^carifilippova@yandex.ru, ^dm.teplonogova@gmail.com, ^evan@igic.ras.ru, ^fantonpopovleonid@gmail.com

Corresponding author: Anton L. Popov, antonpopovleonid@gmail.com

ABSTRACT Cerium fluoride (CeF_3) nanoparticles (NPs), being a unique nanozyme and redox-active nanomaterial, show high promise for advanced biomedical applications. Doping of CeF_3 NPs with the other chemical elements allow one to increase their catalytic activity, impart them new functional properties, and also to increase the efficiency of their interaction with ionizing radiation, which is important in the development of novel nanoradiosensitizers. In this article, we synthesized citrate-stabilized $\text{Ce}_{0.75}\text{Bi}_{0.15}\text{Tb}_{0.1}\text{F}_3$ nanoparticles, which demonstrate high colloidal stability, have good luminescent properties and radiation-induced redox activity. Cytotoxicity analysis of $\text{Ce}_{0.75}\text{Bi}_{0.15}\text{Tb}_{0.1}\text{F}_3$ NPs using normal and tumor cells *in vitro* showed the sensitivity of B16/F10 and EMT6 tumor cell lines to the nanoparticles at high concentrations (0.5 – 1 mM). Obtained experimental results allow us to consider $\text{Ce}_{0.75}\text{Bi}_{0.15}\text{Tb}_{0.1}\text{F}_3$ nanoparticles as a possible platform for the development of a new class of nanoradiosensitizers for radiation therapy purposes.

KEYWORDS nanoparticles, cytotoxicity, fluoride, cerium

ACKNOWLEDGEMENTS The work was supported by the Russian Science Foundation (project no. 22-73-10231, <https://rscf.ru/project/22-73-10231/>).

FOR CITATION Chukavin N.N., Kolmanovich D.D., Filippova A.D., Teplonogova M.A., Ivanov V.K., Popov A.L. Synthesis of redox-active $\text{Ce}_{0.75}\text{Bi}_{0.15}\text{Tb}_{0.1}\text{F}_3$ nanoparticles and their biocompatibility study *in vitro*. *Nanosystems: Phys. Chem. Math.*, 2024, **15** (2), 260–267.

1. Introduction

Nanocrystalline materials based on cerium(IV) oxide are currently widely used in various fields of biomedicine due to their unique catalytic properties and high degree of biocompatibility [1–4]. Due to their redox activity and the ability to mimic the activity of various enzymes, CeO_2 nanoparticles have become the most promising inorganic nanozymes [5–8]. Catalytic activity of these nanoparticles is based on the unique reversible $\text{Ce}^{3+}/\text{Ce}^{4+}$ transition, which determines its role as prooxidant and reactive oxygen species (ROS) generator at low pH values in tumor cells, or as an antioxidant and ROS inactivator under normal physiological pH conditions [9]. Meanwhile, earlier we have demonstrated for the first time the catalytic activity of CeF_3 nanoparticles, the mechanism of action of which differs from that of CeO_2 nanoparticles. We have shown that CeF_3 NPs demonstrate selective cytotoxicity to tumor cells, inhibiting their proliferative activity and DNA repair under X-ray irradiation [10]. Also, we have reported the ability of CeF_3 NPs to stimulate planarian regeneration [11] and to act as an effective radioprotector under X-ray irradiation [12]. In a number of studies, authors have shown that doping of REE fluorides provides them with unique properties [13–17]. Particularly, additional chemical modification of CeF_3 NPs provides them with new functional properties. For instance, doping of CeF_3 crystal lattice with Yb and Tm ions allows for the formation of theranostic luminescent systems with enhanced upconversion ($\text{CeF}_3:\text{Yb}$, $\text{Tm}@\text{SiO}_2\text{-CD36/OPN}$) [18]. Wang et al. synthesized biocompatible $\text{CeF}_3:\text{Tb}@\text{LaF}_3$ NPs with pronounced luminescent properties [19], which could be used for bioimaging, biolabeling, biodetection and bioprobing. $\text{Ce}_x\text{La}_{1-x}\text{F}_3$ NPs have been proposed for the use in nanoscintillator-photosensitizer systems, in which excitation of nanoparticles by ionizing irradiation leads to energy transfer to photosensitizer molecules, effectively combining the effects of radiation and photodynamic therapy [20].

Nanoparticle-based radioenhancement is considered as a promising approach to improve therapeutic effect of radiation therapy [21–23]. Mechanisms of nanoparticle-based radiosensitizers action can include: physical, chemical and

biological. Ionizing radiation leads to the ejection of secondary electrons which can interact with water, causing ROS generation. In turn, ROS interact with different components of the cell, including cell membrane, mRNA, DNA and, consequently, triggering cell death. Thus, the use of nanoparticles based on high-Z elements and on elements with low ionization potential can significantly increase the efficiency of radiation therapy [24–26]. In particular, the drug NBTXR3/Hensify® (Nanobiotix, Paris, France) based on hafnium oxide has already been approved and is being used [27], and the drug AGuIX® (NH TherAguix, Lyon, France) based on gadolinium is undergoing clinical trials [28]. Thus, synthesis and comprehensive analysis of new theranostic agents for radiotherapy is an urgent task.

In this study, we have synthesized citrate-stabilized $Ce_{0.75}Bi_{0.15}Tb_{0.1}F_3$ nanoparticles, analyzed their physico-chemical characteristics and studied their cytotoxicity to normal and tumor cells *in vitro*.

2. Materials and methods

2.1. Synthesis scheme

For the synthesis of $Ce_{0.75}Bi_{0.15}Tb_{0.1}F_3$ colloidal solutions the following substances were used: $Ce(NO_3)_3 \cdot 6H_2O$ (puriss., Lanhit), $Tb(NO_3)_3 \cdot 6H_2O$ (puriss., Lanhit), $Bi(NO_3)_3 \cdot 5H_2O$ (pur., Reachem), HF (puriss. spec., Sigma Tec), ammonium citrate dibasic (puriss., Sigma-Aldrich), isopropanol (puriss. spec., Chimmed), ethylene glycol (puriss., Sigma Aldrich). Samples of rare earth elements (REE) nitrates (1.628 g $Ce(NO_3)_3 \cdot 6H_2O$, 0.228 g $Tb(NO_3)_3 \cdot 6H_2O$, 0.363 g $Bi(NO_3)_3 \cdot 5H_2O$) were suspended in 30 mL of ethylene glycol upon heating to 60 °C and intense stirring on a magnetic stirrer. 0.885 mL of 40 % HF was dissolved in 150 mL of isopropanol. The obtained solution was added drop by drop to mixed REE nitrates solution with intensive stirring until the suspension was formed. The precipitate was separated by filtration through a paper filter (2 – 3 μm), washed with isopropanol, placed in an oven for 30 – 60 minutes at 50 °C to remove isopropanol. Wet gel-like precipitate was re-dispersed in 100 mL of deionized water. Ammonium citrate solution (1.134 g of ammonium citrate in 100 mL of deionized water) was added to the resulting suspension with intense stirring. The resulting sol was mixed at 30 – 35 °C until remnant isopropanol was removed. The concentration of the resulting sol was 7.6 mM.

2.2. Characterization of $Ce_{0.75}Bi_{0.15}Tb_{0.1}F_3$ NPs

Powder X-ray diffraction analysis (XRD) of the samples was carried out on a Haoyuan DX-2700BH diffractometer ($CuK\alpha$ radiation, $\lambda = 1.54184 \text{ \AA}$) in the range of 5 – 60° 2θ with a step of 0.02° and a shutter speed of 1 sec/step. The diffractograms were indexed using the ICDD PDF2 database. The concentration of the $Ce_{0.75}Bi_{0.15}Tb_{0.1}F_3$ NPs sols was determined gravimetrically. The corundum crucibles pre-annealed at 900 °C for 2 hours were weighted on analytical scales to establish their initial weight. Then 3 mL of sol was placed in each crucible and heated in a muffle furnace at 900 °C for 2 hours with slow heating ($\sim 3 \text{ }^\circ/\text{min}$). After cooling to room temperature, the crucibles were weighted. The weight of the dry residue of the annealing product was determined and the concentration of the initial sols was calculated. The study of the elemental composition of the obtained materials was carried out using energy dispersive X-ray spectroscopy (EDX) using a Tescan Amber GMH microscope equipped with an Ultim MAX detector with 100 mm² active area (Oxford Instruments) at an accelerating voltage of 20 kV. EDX data were processed using the AZtec software (5.0). An UV5 Nano spectrophotometer (Mettler Toledo, Columbus, Ohio, USA) was used to measure $Ce_{0.75}Bi_{0.15}Tb_{0.1}F_3$ NPs sols absorbance in the UV-visible range. Measurements were carried out in the wavelength range from 200 to 600 nm in 0.1 nm increments. The sizes and ζ -potentials of nanoparticles were determined by dynamic and electrophoretic light scattering at 25 °C using a BeNano analyzer (BetterSize, Dandong, China).

2.3. Cell culture

The experiments were performed using 5 types of cell cultures: B16F10 (murine melanoma), EMT6/P (murine adenocarcinoma), MNNG/HOS (human osteosarcoma), MCF-7 (human adenocarcinoma), NCTC L929 (murine fibroblasts) obtained from Theranostics and Nuclear Medicine Laboratory cryostorage (ITEB RAS, Pushchino, Russia). The cells were cultured in a DMEM/F12 (1:1) culture medium containing 50 $\mu g/mL$ of penicillin, 50 $\mu g/mL$ of streptomycin, 10 % of fetal bovine serum (FBS) and 1 % of L-glutamine at a temperature of 37 °C in a 95 % humidity atmosphere containing 95 % air and 5 % CO₂. The cells were seeded on 96-well plates at a density of 25000 cells/cm². 6 hours after cell attachment the culture medium was then replaced with a fresh culture medium containing different concentrations of $Ce_{0.75}Bi_{0.15}Tb_{0.1}F_3$ NPs (0.1 – 1 mM). Cells from the control groups were cultured without the addition of $Ce_{0.75}Bi_{0.15}Tb_{0.1}F_3$ NPs.

2.4. MTT assay

Cell viability was assessed using MTT assay which is based on the reduction of a yellow tetrazolium salt (3-[4,5-dimethylthiazole-2-yl]-2,5-diphenyl tetrazolium bromide, MTT) to insoluble formazan crystals having purple color. After 48 hours of cultivation, 0.5 mg/mL MTT reagent solution, dissolved in culture medium without FBS, was added to the wells. The optical density of the formed formazan was measured at $\lambda = 570 \text{ nm}$ using an INNO-S plate reader (LTEK, Korea).

2.5. Live/Dead assay

The cytotoxic effect of $\text{Ce}_{0.75}\text{Bi}_{0.15}\text{Tb}_{0.1}\text{F}_3$ NPs was assessed using a Live/Dead assay. This method is based on measuring the percentage of dead cells to their total number after their incubation with $\text{Ce}_{0.75}\text{Bi}_{0.15}\text{Tb}_{0.1}\text{F}_3$ NPs. Cells were labeled via staining with a combination of the fluorescent dyes Hoechst 33342 (binds to DNA of all cells, $\lambda_{ex} = 350$ nm, $\lambda_{em} = 460$ nm) and propidium iodide (binds to DNA of dead cells, $\lambda_{ex} = 535$ nm, $\lambda_{em} = 615$ nm). After 24, 48, and 72 hours of incubation with nanoparticles, the culture medium was replaced with a mixture of Hoechst 33342 and propidium iodide in Hanks' buffer solution (PanEko, Moscow, Russia). After 15 min of incubation with dyes, the cells were washed three times with Hanks' buffer solution. Then, cells were photographed using a ZOE fluorescent imager (Bio-Rad, USA). ImageJ software was used to count the number of cells. Three different cell areas on the field were analyzed on three different microphotographs. Quantitative analysis results were presented as mean \pm SD.

2.6. Measuring of mitochondrial membrane potential

The mitochondrial membrane potential (MMP) was measured by staining cells with TMRE (tetramethylrhodamine, ethyl ester, ThermoFisher, Carlsbad, CA, USA) fluorescent dye followed by fluorescence microscopy analysis. After 24, 48, and 72 hours of incubation with nanoparticles, the culture medium was replaced with TMRE solution in Hanks' buffer (PanEko, Moscow, Russia). After 15 min of incubation with dye, the cells were washed three times with Hanks' buffer solution. Then, the cells were photographed using a ZOE fluorescent imager (Bio-Rad, USA). TMRE fluorescence intensity, which directly correlates with the MMP of cells, was measured using the ImageJ software. Three different areas on the field were analyzed on three different microphotographs. Quantitative analysis results were presented as mean \pm SD.

2.7. Statistical analysis

Three independent experiments with three independent repetitions for each $\text{Ce}_{0.75}\text{Bi}_{0.15}\text{Tb}_{0.1}\text{F}_3$ NPs concentration were performed. Experimental results were compared with untreated control. Statistical analysis was performed using the methods of variation statistics (ANOVA, Student's t-test). The mean values and the standard deviations (SD) were determined. The obtained data were processed using the GraphPad Prism 8.0 software.

3. Results and discussion

The scheme of $\text{Ce}_{0.75}\text{Bi}_{0.15}\text{Tb}_{0.1}\text{F}_3$ NPs synthesis is shown in Fig. 1a. EDX analysis confirms the elemental composition of the nanoparticles, where the peaks of cerium, bismuth and terbium are easily discernible (Fig. 1b). Quantitative EDX analysis revealed the following cation ratios: Ce : Bi : Tb = 79 : 14 : 7. Fig. 1c shows a fluorescence spectrum of the $\text{Ce}_{0.75}\text{Bi}_{0.15}\text{Tb}_{0.1}\text{F}_3$ NPs, Fig. 1d shows the UV-visible absorption spectrum of $\text{Ce}_{0.75}\text{Bi}_{0.15}\text{Tb}_{0.1}\text{F}_3$ NPs. The spectrum contains characteristic absorption peaks of Ce^{3+} ions (245 nm) and citric acid (225 nm), which confirms the presence of these components in the composition of nanoparticles. The diffraction pattern of $\text{Ce}_{0.75}\text{Bi}_{0.15}\text{Tb}_{0.1}\text{F}_3$ NPs corresponds well to the structure of CeF_3 (PDF2 card No. 8-45), however, due to the significant broadening of diffraction maxima, it is not possible to clarify the unit cell parameters (Fig. 1e). The significant broadening of diffraction maxima of $\text{Ce}_{0.75}\text{Bi}_{0.15}\text{Tb}_{0.1}\text{F}_3$ NPs confirms the small size of the nanoparticles. The distribution of the hydrodynamic diameters of $\text{Ce}_{0.75}\text{Bi}_{0.15}\text{Tb}_{0.1}\text{F}_3$ NPs in water indicates the polydispersity of these nanoparticles (PDI = 0.238) (Fig. 1f). Analysis of the ζ -potential of $\text{Ce}_{0.75}\text{Bi}_{0.15}\text{Tb}_{0.1}\text{F}_3$ NPs indicates the colloidal stability of the aqueous sol of these nanoparticles (ζ -potential -36 mV) (Fig. 1g).

Routine MTT assay was used to study $\text{Ce}_{0.75}\text{Bi}_{0.15}\text{Tb}_{0.1}\text{F}_3$ NPs cytotoxicity. The NAD(P)H-dependent cytosolic oxidoreductases activity measured during MTT assay is associated with the metabolic activity of cells, which, in turn, is one of the main indicators of cell viability [29]. According to the results of the study of the metabolic activity of B16F10, EMT6/P, MNNG/HOS, MCF-7, NCTC L929 cell cultures, the pronounced dose-dependent effect was revealed after 24 hours of coincubation of the cells with $\text{Ce}_{0.75}\text{Bi}_{0.15}\text{Tb}_{0.1}\text{F}_3$ NPs (Fig. 2). It was shown that the viability of B16/F10, EMT6/P, MNNG/HOS and MCF-7 cells decreased by 25 %, while NCTC L929 cells viability decreased by 50 % after 24 hours of incubation with $\text{Ce}_{0.75}\text{Bi}_{0.15}\text{Tb}_{0.1}\text{F}_3$ NPs at a 1 mM concentration. Moreover, the viability of B16/F10, EMT6/P and NCTC L929 cells decreased by 75 % after 72 hours of incubation with 1 mM $\text{Ce}_{0.75}\text{Bi}_{0.15}\text{Tb}_{0.1}\text{F}_3$ NPs. MCF-7 and MNNG/HOS cells were found to be the most resistant cell lines to cytotoxic effect of $\text{Ce}_{0.75}\text{Bi}_{0.15}\text{Tb}_{0.1}\text{F}_3$ NPs.

According to the measured live/dead cells ratios (Fig. 3), the pronounced cytotoxic effect of $\text{Ce}_{0.75}\text{Bi}_{0.15}\text{Tb}_{0.1}\text{F}_3$ NPs was revealed on EMT6/P, MCF-7 and NCTC L929 cell lines after 72 hours of incubation with these nanoparticles. This effect consisted in an increase in the percentage of dead cells. The maximum percentage of dead cells was about 50 % at a $\text{Ce}_{0.75}\text{Bi}_{0.15}\text{Tb}_{0.1}\text{F}_3$ NPs concentration of 1 mM. However, nanoparticles showed significantly lower cytotoxicity to B16/F10 and MNNG/HOS cells (20 % cell death). Thus, it can be concluded that the cell viability decrease caused by $\text{Ce}_{0.75}\text{Bi}_{0.15}\text{Tb}_{0.1}\text{F}_3$ NPs does not necessarily lead to the development of apoptosis and cell death, as it has been shown for mouse melanoma cells. The revealed differences in the behavior of the cells may also be due to the different efficiency of endocytosis of this type of nanoparticles, which directly correlates with their effect on cell viability.

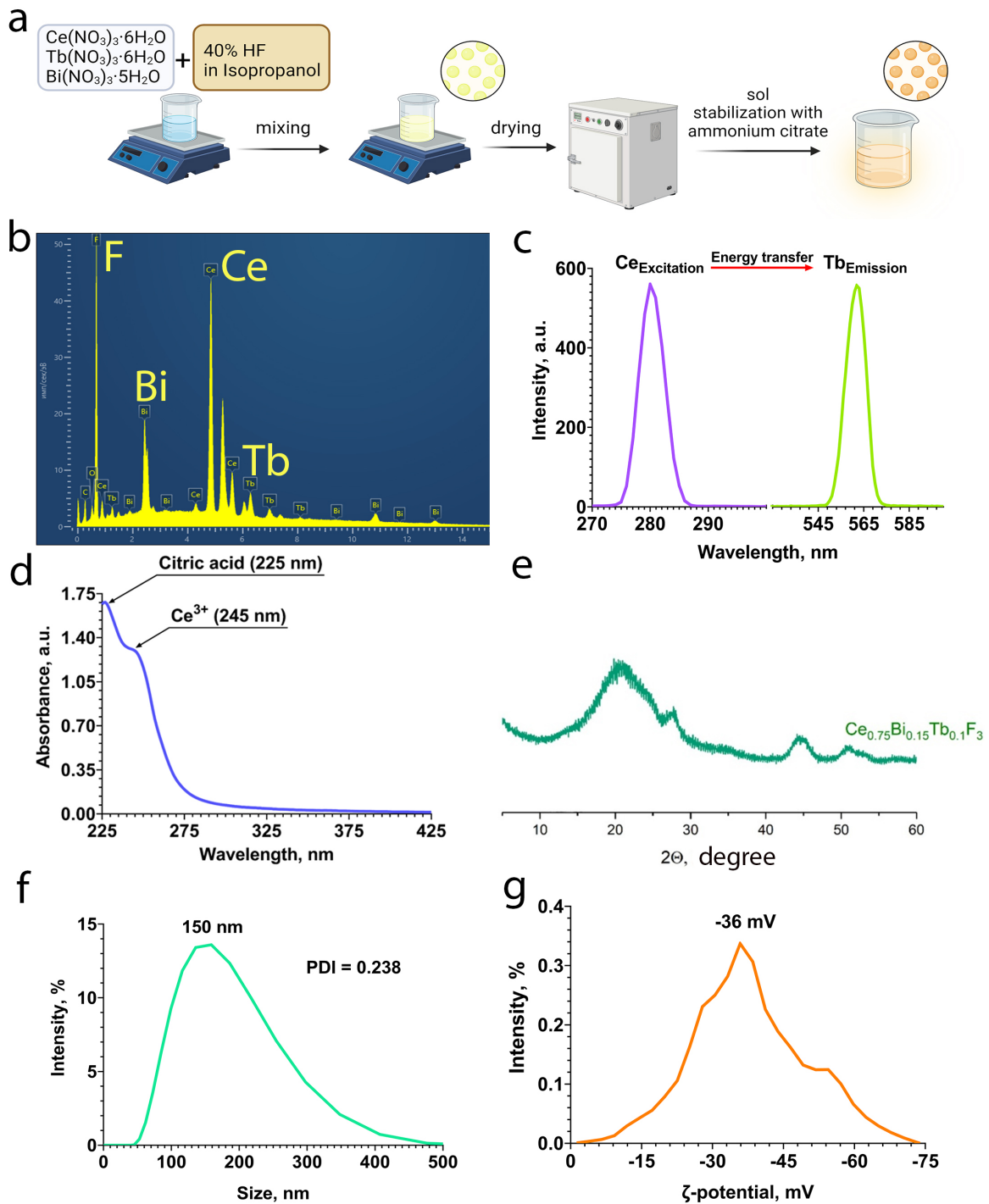


FIG. 1. Synthesis scheme (a), EDX spectrum (b), fluorescence spectrum (c), UV-visible absorbance spectrum (d), diffraction pattern (e), hydrodynamic diameter distribution (f) and ζ -potential distribution (g) of the $Ce_{0.75}Bi_{0.15}Tb_{0.1}F_3$ NPs

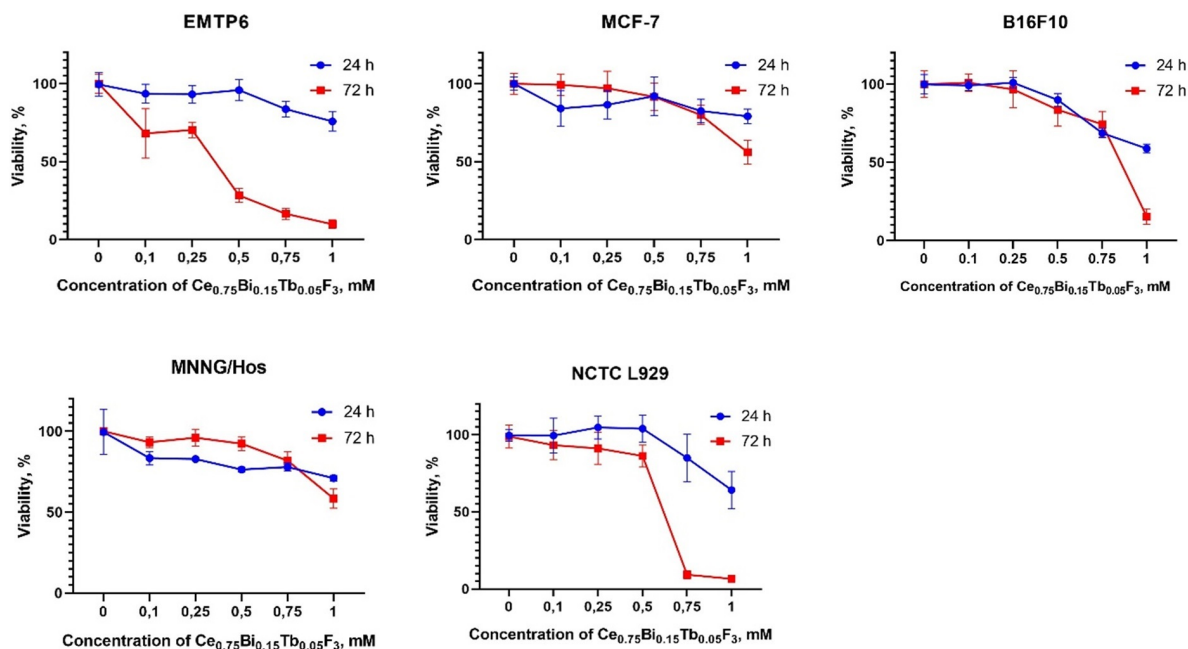


FIG. 2. Viability of cancer (B16F10, EMTP6, MCF-7, MNNG/HOS) and normal (NCTC L929) cells according to MTT assay. The cells were incubated with $Ce_{0.75}Bi_{0.15}Tb_{0.1}F_3$ NPs (0.1–1 mM) for 24 and 72 hours

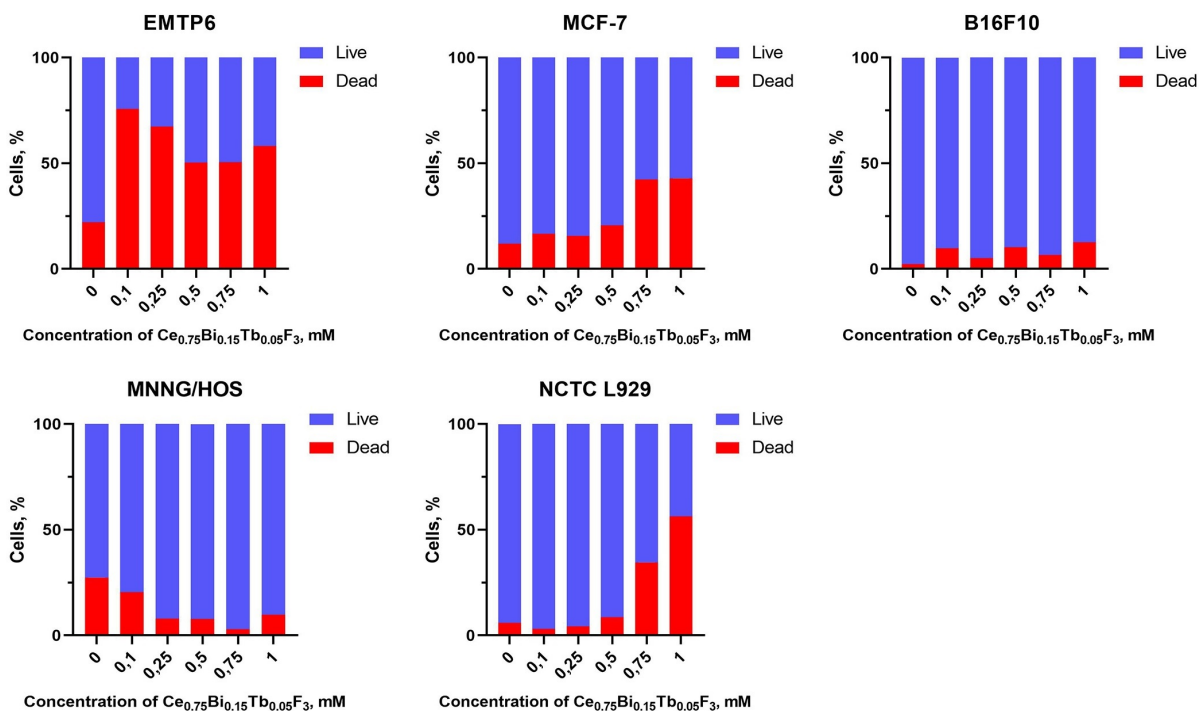


FIG. 3. Ratios of live/dead cancer (B16/F10, EMTP6/P, MCF-7, MNNG/HOS) and normal (NCTC L929) cells after 72 hours of incubation with $Ce_{0.75}Bi_{0.15}Tb_{0.1}F_3$ NPs (0.1 – 1 mM)

Using fluorescent tetramethylrhodamine (TMRE) dye, which is accumulated in mitochondria in a voltage-dependent manner, we analyzed the mitochondrial membrane potential (MMP) of cell cultures after 72 hours of incubation with $Ce_{0.75}Bi_{0.15}Tb_{0.1}F_3$ NPs (Fig. 4). The significant decrease of MMP in the presence of nanoparticles was shown for human osteosarcoma MMNG/HOS and human adenocarcinoma MCF-7 cells. In addition, the pronounced cytotoxic effect of $Ce_{0.75}Bi_{0.15}Tb_{0.1}F_3$ NPs in the form of a dose-dependent MMP decrease was revealed for normal murine fibroblasts. Oppositely, MMP of murine melanoma B16/F10 cells did not change significantly after incubation with nanoparticles in the entire studied concentrations range (0.1 – 1 mM). The redox activity of cerium-containing nanoparticles can lead to mitochondrial dysfunction in tumor cells. In particular, Aplak et al. demonstrated, using human melanoma A375 cells, that cerium dioxide nanoparticles initiate an increase of mitochondrial ROS levels accompanied by an increase in mitochondrial thiol oxidation [30]. Also, the authors revealed changes in mitochondrial bioenergetics and crista morphology that led to the death of tumor cells.

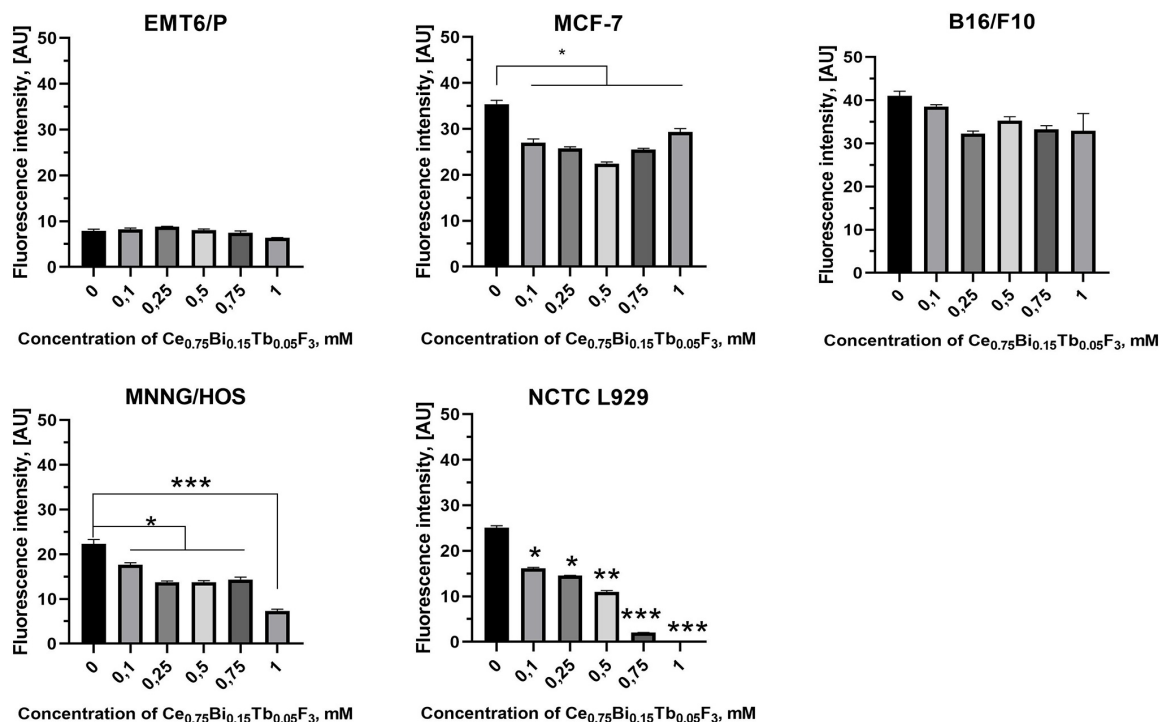


FIG. 4. Quantitative assessment of the mitochondrial membrane potential (MMP) of cancer (B16F10, EMT6/P, MCF-7, MNNG/HOS) and normal (NCTC L929) cells after 72 hours of incubation with $Ce_{0.75}Bi_{0.15}Tb_{0.1}F_3$ NPs at a concentration of 0.1 – 1 mM. Cells were stained with TMRE. Mean \pm standard deviation (SD) is plotted for five replicates, * $p < 0.05$, ** $p < 0.01$, *** $p < 0.005$

Analysis of the $Ce_{0.75}Bi_{0.15}Tb_{0.1}F_3$ NPs redox-activity under X-ray irradiation in aqueous solution was performed using the method of enhanced chemiluminescence in the iodophenol-horseradish peroxidase system (Fig. 5a). High sensitivity of this method makes it possible to determine changes in hydrogen peroxide concentrations up to 1 nM. X-ray irradiation (1 Gy) of the control group (solution without NPs) led to the formation of about 80 nM of hydrogen peroxide (Fig. 5b). $Ce_{0.75}Bi_{0.15}Tb_{0.1}F_3$ NPs colloidal solution (0.5 mM) demonstrated prooxidant activity which was expressed in a twofold increase in the level of hydrogen peroxide after irradiation at a dose of 1 Gy. This effect was observed regardless of the pH value of the colloidal solution.

Earlier, we have shown that cerium fluoride nanoparticles, including those doped with REE (for example, gadolinium), exhibit prooxidant activity under acidic pH conditions [31]. Thus, irradiation of tumor cells, containing $Ce_{0.75}Bi_{0.15}Tb_{0.1}F_3$ NPs, would lead to enhanced intracellular ROS generation, resulting in an accelerated radiation-induced cell death.

4. Conclusions

Citrate-stabilized $Ce_{0.75}Bi_{0.15}Tb_{0.1}F_3$ nanoparticles were synthesized by a facile precipitation technique. Analysis of the $Ce_{0.75}Bi_{0.15}Tb_{0.1}F_3$ NPs confirmed the composition and structure of these nanoparticles, as well as their good luminescent properties due to the presence of terbium ions in the crystal lattice of nanoparticles. $Ce_{0.75}Bi_{0.15}Tb_{0.1}F_3$ NPs at a concentration of 0.5 – 1 mM exhibit different cytotoxicity to normal and tumor cell lines, suppressing their

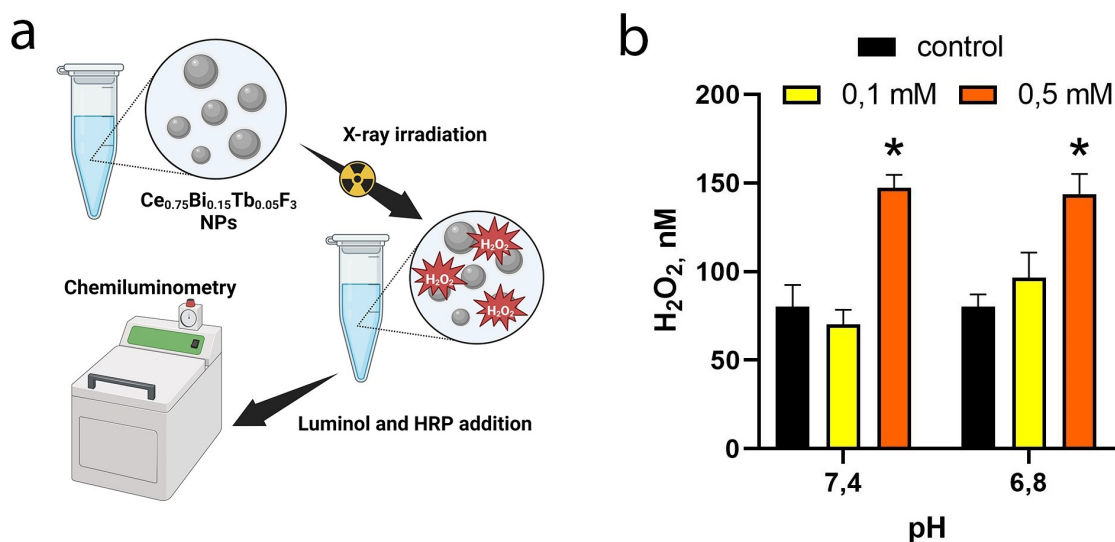


FIG. 5. Redox activity of $\text{Ce}_{0.75}\text{Bi}_{0.15}\text{Tb}_{0.1}\text{F}_3$ NPs under X-ray irradiation (1 Gy). Schematic representation of the experiment (a). Concentration of hydrogen peroxide after X-ray irradiation (total dose 1 Gy) of the $\text{Ce}_{0.75}\text{Bi}_{0.15}\text{Tb}_{0.1}\text{F}_3$ NPs colloid solution at pH 6.8 and pH 7.2 (b). The level of hydrogen peroxide was determined by the chemiluminescent method, using iodophenol-horseradish peroxidase system

viability and MMP and contributing to their death. Radiation-induced redox activity of $\text{Ce}_{0.75}\text{Bi}_{0.15}\text{Tb}_{0.1}\text{F}_3$ NPs was revealed upon X-ray irradiation that confirms the possibility of their application as a radiosensitizer in various tumor models *in vitro* and *in vivo*.

References

- [1] Tang J.L.Y., Moonshi S.S., Ta H.T. Nanoceria: An Innovative Strategy for Cancer Treatment. *Cell. Mol. Life Sci.*, 2023, **80**, 46.
- [2] Li H., Xia P., Pan S., Qi Z., Fu C., Yu Z., Kong W., Chang Y., Wang K., Wu D., et al. The Advances of Ceria Nanoparticles for Biomedical Applications in Orthopaedics. *Int. J. Nanomedicine*, 2020, **15**, P. 7199–7214.
- [3] Garzón-Manjón A., Aranda-Ramos A., Melara-Benítez B., Bensarghin I., Ros J., Ricart S., Nogués C. Simple Synthesis of Biocompatible Stable CeO_2 Nanoparticles as Antioxidant Agents. *Bioconjug. Chem.*, 2018, **29**, P. 2325–2331.
- [4] Banavar S., Deshpande A., Sur S., Andreescu S. Ceria Nanoparticle Theranostics: Harnessing Antioxidant Properties in Biomedicine and Beyond. *J. Phys. Mater.*, 2021, **4**, 042003
- [5] Popov A.L., Shcherbakov A.B., Zhlobak N.M., Baranchikov A.E., Ivanov V.K. Cerium Dioxide Nanoparticles as Third-Generation Enzymes (Nanozymes). *Nanosyst. Phys. Chem. Math.*, 2017, **8** (6), P. 760–781.
- [6] Liu H., Liu J. Self-Limited Phosphatase-Mimicking CeO_2 Nanozymes. *ChemNanoMat*, 2020, **6**, P. 947–952.
- [7] Ma Y., Tian Z., Zhai W., Qu Y. Insights on Catalytic Mechanism of CeO_2 as Multiple Nanozymes. *Nano Res.*, 2022, **15**, P. 10328–10342.
- [8] Luo Q., Li Y., Huo X., Li J., Li L., Wang W., Li Y., Chen S., Song Y., Wang N. Stabilizing Ultrasmall Ceria-Cluster Nanozyme for Antibacterial and Antibiofouling Applications. *Small*, 2022, **18**, 2107401.
- [9] Nelson B.C., Johnson M.E., Walker M.L., Riley K.R., Sims C.M. Antioxidant Cerium Oxide Nanoparticles in Biology and Medicine. *Antioxidants*, 2016 **5**, 15.
- [10] Chukavin N.N., Filippova K.O., Ermakov A.M., Karmanova E.E., Popova N.R., Anikina V.A., Ivanova O.S., Ivanov V.K., Popov A.L. Redox-Active Cerium Fluoride Nanoparticles Selectively Modulate Cellular Response against X-Ray Irradiation In Vitro. *Biomedicines*, 2024, **12**, 11.
- [11] Ermakov A., Popov A., Ermakova O., Ivanova O., Baranchikov A., Kamenskikh K., Shekunova T., Shcherbakov A., Popova N., Ivanov V. The First Inorganic Mitogens: Cerium Oxide and Cerium Fluoride Nanoparticles Stimulate Planarian Regeneration via Neoblastic Activation. *Mater. Sci. Eng. C*, 2019, **104**, 109924.
- [12] Filippova K.O., Ermakov A.M., Popov A.L., Ermakova O.N., Blagodatsky A.S., Chukavin N.N., Shcherbakov A.B., Baranchikov A.E., Ivanov V.K. Mitogen-like Cerium-Based Nanoparticles Protect Schmidtea Mediterranea against Severe Doses of X-Rays. *Int. J. Mol. Sci.*, 2023, **24**, 1241.
- [13] Jacobsohn L.G., Kucera C.J., James T.L., Sprinkle K.B., DiMaio J.R., Kokuoz B., Yazgan-Kukouoz B., DeVol T.A., Ballato J. Preparation and Characterization of Rare Earth Doped Fluoride Nanoparticles. *Materials*, 2010, **3**, P. 2053–2068.
- [14] Secco H. de L., Ferreira F.F., Péres L.O. Simple Preparation of Fluorescent Composite Films Based on Cerium and Europium Doped LaF_3 Nanoparticles. *J. Solid State Chem.*, 2018, **259**, P. 43–47.
- [15] Huang D.T.M., Tien N.T., Vu L.V., Long N.N. Synthesis and Optical Characterization of Samarium Doped Cerium Fluoride Nanoparticles. *VNU J. Sci. Math.-Phys.*, 2015, **31**.
- [16] Greis O., Haschke J.M. Rare Earth Fluorides. In *Handbook on the Physics and Chemistry of Rare Earths*, Elsevier, 1982, **5**, P. 387–460.
- [17] Pudovkin M.S., Morozov O.A., Korableva S.L., Rakhmatullin R.M., Semashko V.V., Ginkel A.K., Rodionov A.A., Kiiamov A.G. EPR and Optical Study of Erbium-Doped CeO_2 and $\text{CeO}_2/\text{CeF}_3$ Nanoparticles. *Ceram. Int.*, 2024, **50**, P. 9263–9269.
- [18] Cheng Y., Xu H., Cao W., Gao W., Tang B. Cerium Fluoride Nanoparticles as a Theranostic Material for Optical Imaging of Vulnerable Atherosclerosis Plaques. *J. Am. Ceram. Soc.*, 2023, **106**, P. 2375–2383.
- [19] Wang J., Ansari A.A., Malik A., Syed R., Ola M.S., Kumar A., AlGhamdi K.M., Khan S. Highly Water-Soluble Luminescent Silica-Coated Cerium Fluoride Nanoparticles Synthesis, Characterizations, and In Vitro Evaluation of Possible Cytotoxicity. *ACS Omega*, 2020, **5**, P. 19174–19180.

- [20] Cooper D.R., Kudinov K., Tyagi P., Hill C.K., Bradforth S.E., Nadeau J.L. Photoluminescence of Cerium Fluoride and Cerium-Doped Lanthanum Fluoride Nanoparticles and Investigation of Energy Transfer to Photosensitizer Molecules. *Phys. Chem. Chem. Phys.*, 2014, **16**, P. 12441–12453.
- [21] Gerken L.R.H., Gerdes M.E., Pruschy M., Herrmann I.K. Prospects of Nanoparticle-Based Radioenhancement for Radiotherapy. *Mater. Horiz.*, 2023, **10**, P. 4059–4082.
- [22] Deng J., Xu S., Hu W., Xun X., Zheng L., Su M. Tumor Targeted Stealthy and Degradable Bismuth Nanoparticles for Enhanced X-Ray Radiation Therapy of Breast Cancer. *Biomaterials*, 2018, **154**, P. 24–33.
- [23] Fan W., Tang W., Lau J., Shen Z., Xie J., Shi J., Chen X. Breaking the Depth Dependence by Nanotechnology-Enhanced X-Ray-Excited Deep Cancer Theranostics. *Adv. Mater.*, 2019, **31**, 1806381.
- [24] Yuan Z., Liu X., Ling J., Huang G., Huang J., Zhu X., He L., Chen T. In Situ-Transition Nanozyme Triggered by Tumor Microenvironment Boosts Synergistic Cancer Radio-/Chemotherapy through Disrupting Redox Homeostasis. *Biomaterials*, 2022, **287**, 121620.
- [25] Liu S., Fang L., Ding H., Zhang Y., Li W., Liu B., Dong S., Tian B., Feng L., Yang P. Alternative Strategy to Optimize Cerium Oxide for Enhanced X-Ray-Induced Photodynamic Therapy. *ACS Nano*, 2022, **16**, P. 20805–20819.
- [26] Zhu X., Wu J., Liu R., Xiang H., Zhang W., Chang Q., Wang S., Jiang R., Zhao F., Li Q., et al. Engineering Single-Atom Iron Nanozymes with Radiation-Enhanced Self-Cascade Catalysis and Self-Supplied H₂O₂ for Radio-Enzymatic Therapy. *ACS Nano*, 2022, **16**, P. 18849–18862.
- [27] Bagley A.F., Ludmir E.B., Maitra A., Minsky B.D., Li Smith G., Das P., Koong A.C., Holliday E.B., Taniguchi C.M., Katz M.H.G., et al. NBTXR3, a First-in-Class Radioenhancer for Pancreatic Ductal Adenocarcinoma: Report of First Patient Experience. *Clin. Transl. Radiat. Oncol.*, 2022, **33**, P. 66–69.
- [28] Lux F., Tran V.L., Thomas E., Dufort S., Rossetti F., Martini M., Truillet C., Doussineau T., Bort G., Denat F., et al. AGuIX® from Bench to Bedside-Transfer of an Ultrasmall Theranostic Gadolinium-Based Nanoparticle to Clinical Medicine. *Br. J. Radiol.*, 2019, **92**, 20180365.
- [29] Ghasemi M., Turnbull T., Sebastian S., Kempson I. The MTT Assay: Utility, Limitations, Pitfalls, and Interpretation in Bulk and Single-Cell Analysis. *Int. J. Mol. Sci.*, 2021, **22**, 12827.
- [30] Aplak E., Montfort C. von, Haasler L., Stucki D., Steckel B., Reichert A.S., Stahl W., Brenneisen P. CNP Mediated Selective Toxicity on Melanoma Cells Is Accompanied by Mitochondrial Dysfunction. *PLOS ONE*, 2020, **15**, e0227926.
- [31] Kolmanovich D.D., Chukavin N.N., Savintseva I.V., Mysina E.A., Popova N.R., Baranchikov A.E., Sozarukova M.M., Ivanov V.K., Popov A.L. Hybrid Polyelectrolyte Capsules Loaded with Gadolinium-Doped Cerium Oxide Nanoparticles as a Biocompatible MRI Agent for Theranostic Applications. *Polymers*, 2023, **15**, 3840.

Submitted 15 January 2024; accepted 28 February 2024

Information about the authors:

Nikita N. Chukavin – Institute of Theoretical and Experimental Biophysics of the Russian Academy of Sciences, 142290, Russia; ORCID 0000-0001-8431-4485; chukavinnik@gmail.com

Danil D. Kolmanovich – Institute of Theoretical and Experimental Biophysics of the Russian Academy of Sciences, 142290, Russia; ORCID 0000-0003-3391-7889; kdd100996@mail.ru

Arina D. Filippova – Kurnakov Institute of General and Inorganic Chemistry of the Russian Academy of Sciences, Moscow, 119991, Russia; ORCID 0000-0002-2725-8891; arifilippova@yandex.ru

Maria A. Teplonogova – Kurnakov Institute of General and Inorganic Chemistry of the Russian Academy of Sciences, Moscow, 119991, Russia; ORCID 0000-0002-4820-8498; m.teplonogova@gmail.com

Vladimir K. Ivanov – Kurnakov Institute of General and Inorganic Chemistry of the Russian Academy of Sciences, Moscow, 119991, Russia; ORCID 0000-0003-2343-2140; van@igic.ras.ru

Anton L. Popov – Institute of Theoretical and Experimental Biophysics of the Russian Academy of Sciences, 142290, Russia; ORCID 0000-0003-2643-4846; antonpopovleonid@gmail.com

Conflict of interest: the authors declare no conflict of interest.